SARS Coronavirus ORF7a inhibits BST-2 virion tethering through a novel mechanism of glycosylation interference

Justin K. Taylor[a], Christopher M. Coleman[a], Sandra Postel[b], Jeanne M. Sisk[a], John G. Bernbaum[c], Thiagarajan Venkatarajan[a], Eric J. Sundberg[a,b,d], Matthew B. Frieman[a]#

Department of Microbiology and Immunology, University of Maryland at Baltimore, Baltimore, Maryland, USA[a]; Institute of Human Virology, University of Maryland School of Medicine, Baltimore, Maryland, USA[b]; and Integrated Research Facility, National Institutes of Health, Frederick, Maryland, USA[c]; Department of Medicine, University of Maryland School of Medicine, Baltimore, Maryland, USA[d]

Running Head: BST-2 restricts SARS-coronavirus

#Address correspondence to Matthew B. Frieman, mfrieman@som.umaryland.edu.

Abstract

Severe Acute Respiratory Syndrome (SARS) emerged in November 2002 as a case of atypical pneumonia in China and the causative agent of SARS was identified as a novel coronavirus, severe acute respiratory syndrome coronavirus (SARS-CoV). Bone marrow stromal antigen 2 (BST-2; also known as CD317 or tetherin) was initially identified as a pre-B-cell growth promoter but also inhibits the release of the retrovirus human immunodeficiency virus type 1 (HIV-1) virions by tethering budding virions to the host cell membrane. Further work has shown that BST-2 restricts the release of many other viruses, including the human coronavirus hCoV-229E, and many of these viruses encode BST-2 antagonists to overcome BST-2 restriction. Given the previous studies on BST-2, we aimed to determine if BST-2 has the ability to restrict SARS-CoV and if SARS-CoV encodes any proteins that modulate BST-2's anti-viral function. Through an *in vitro* screen we identified four potential BST-2 modulators encoded by SARS-CoV: PL_{Pro}, nsp1, ORF6, and ORF7a. As the function of ORF7a in SARS-CoV replication was previously unknown, we focused our study on ORF7a. We found that BST-2 does restrict SARS-CoV, but the loss of ORF7a leads to a much greater restriction, confirming the role of ORF7a as an inhibitor of BST-2. We further characterized the mechanism of BST-2 inhibition by ORF7a and found that ORF7a localization changes when BST-2 is overexpressed and ORF7a binds directly to BST-2. Finally, we also show that SARS-CoV ORF7a blocks the restriction activity of BST-2 by blocking with the glycosylation of BST-2.

47 **Importance**

48 The severe acute respiratory syndrome coronavirus (SARS-CoV) emerged from
49 zoonotic sources in 2002 and caused over 8000 infections and 800 deaths in 32
50 countries around the world. Identifying host factors that regulate SARS-CoV
51 pathogenesis is critical to understanding how this lethal virus causes disease. We
52 have found that BST-2 is capable of restricting SARS-CoV release from cells,
53 however we also identified a SARS-CoV protein that inhibits BST-2 function. We
54 show that the SARS-CoV protein, ORF7a, inhibits BST-2 glycosylation leading to loss
55 of BST-2's anti-viral function.

56

57 **Introduction**

58 Severe acute respiratory syndrome coronavirus (SARS-CoV) was identified as the
59 causative agent of a 2003 outbreak of severe respiratory disease in the Guangdong
60 province of China resulting in 8096 cases, with 774 deaths, across 29 countries(1, 2).
61 SARS-CoV is an enveloped virus with a positive-sense, single stranded RNA genome
62 of roughly 30,000 nucleotides, encoding four structural proteins: spike (S), envelope
63 (E), membrane (M), and nucleocapsid (N)(3). N protein forms the nucleocapsid,
64 while E and M are minor virion membrane proteins. SARS-CoV entry into the cell is
65 mediated by S protein binding to angiotensin-converting enzyme 2 (ACE2) on the
66 cell surface(4). In addition to the structural proteins, SARS-CoV encodes several
67 non-structural and accessory proteins that promote SARS-CoV replication and
68 virulence(5). Some of the non-structural and accessory proteins function as outside
69 of replication as type-I interferon antagonists(6-8).

ORF7a is a SARS-CoV encoded accessory protein that is composed of a type I transmembrane protein that localizes primarily to the Golgi but can be found on the cell surface (9, 10). SARS-CoV ORF7a overlaps ORF7b in the viral genome where they share a transcriptional regulatory sequence (TRS). ORF7a has a 15 amino acid (aa) N-terminal signal peptide, an 81 aa luminal domain, a 21 aa transmembrane domain and a 5 aa cytoplasmic tail (9, 10). To investigate the role of ORF7a in SARS-CoV replication, an ORF7ab deletion virus was produced that replicated to similar titer as wildtype SARS-CoV *in vitro* and *in vivo*(10-12). Characterization of ORF7a *in vitro* demonstrated ORF7a-dependent induction of apoptosis in a caspase-dependent pathway(13-15). Analysis of ORF7a evolution during the SARS-CoV outbreak identified several residues in ORF7a that were under positive selection as SARS-CoV evolved during transmission from bat to palm civet to humans(16). These data suggest that ORF7a is vital for SARS-CoV biology and has a yet unidentified role in pathogenesis and disease.

Bone marrow stromal antigen 2 (BST-2; also known as CD317 or tetherin) was initially identified as a pre-B-cell growth promoter(17, 18). However, BST-2 is also a marker of type-I interferon producing cells (IPC) and is broadly expressed in many cell types when treated with type-I interferon(19). BST-2 has an unusual structure, with an N-terminal transmembrane domain and a C-terminal glycosylphosphatidylinositol (GPI) anchor and two *N*-linked glycosylation sites in its extracellular domain and exists as a disulfide-linked homodimer(20, 21). BST-2 traffics through the endoplasmic reticulum (ER) and Golgi, eventually localizing to the surface and *trans*-Golgi network(20). Studies have shown evolutionary

conservation in three major surface patches of BST-2, near each of the two *N*-linked glycosylation sites and in the C-terminal region(22).

The anti-viral effect of BST-2 was first identified when it was shown that BST-2 inhibits the release of the retrovirus human immunodeficiency virus type 1 (HIV-1) virions by directly tethering budding virions to the host cell. BST-2 also restricts the release of many other viruses, including alphaviruses, arenaviruses, herpesviruses, paramyxoviruses and other retroviruses(23-26). BST-2 is thought to restrict virus release by physically tethering the budding enveloped virion to the plasma membrane(27) and a number of mechanism models have been proposed (28, 29). All of the BST-2 restriction models predict that BST-2 functions as a dimer, interfacing through ectodomains that incorporate into both the viral envelope and plasma membrane, however models vary in regards to the orientation of the GPI anchor and transmembrane domain. BST-2 has not been shown to interact with any specific viral surface protein, but rather functions as an embedded inter-membrane physical tether. Therefore, BST-2 is thought to be able to restrict any membrane-budding enveloped virus(28, 29). Previous studies have shown that the ability to form cysteine-linked dimers is necessary for BST-2 function, while conflicting results concerning the importance of the *N*-linked glycosylation have been reported(29, 30). More recently, it has been suggested that BST-2 is a virus sensor during HIV-1 infection and induces a proinflammatory response through NFκB(31).

Given the lack of virus specificity in BST-2 restriction, numerous viruses encode BST-2 antagonists to allow release of virions. The first such antagonist was identified as HIV-1 accessory protein Vpu (27). HIV-1 Vpu binds BST-2 and causes β-

116 TrCP2-dependent degradation of BST-2 and efficient release of HIV-1 virions,
117 although it is not clear whether degradation occurs in the lysosome or
118 proteasome(32-34). Other viral antagonists of BST-2 include Chikungunya virus
119 nsp1, ebolavirus GP1,2, herpes simplex virus GP M, HIV-2 envelope glycoprotein,
120 Sendai virus glycoproteins, and simian immunodeficiency virus (SIV) nef and
121 envelope glycoproteins(23-26, 35-38). HIV-2 and SIV are closely related to HIV-1,
122 however, the envelope glycoproteins from HIV-2 and SIV antagonize BST-2 by
123 sequestration within the *trans*-Golgi network rather than degradation, suggesting
124 that different mechanisms of BST-2 antagonism exist for different viruses, even
125 within the same virus genus(35, 36). Another example is Ebolavirus GP1,2 which
126 antagonizes BST-2 through an unknown mechanism that does not involve surface
127 removal but still leads to BST-2 functional inhibition(39).

128 Unlike many enveloped viruses, which bud from the cell plasma membrane,
129 coronaviruses bud in the ER-Golgi intermediate compartment (ERGIC) and are
130 transported to the plasma membrane inside vesicles(40). However, it has recently
131 been shown that BST-2 restricts release to human coronavirus (hCoV)-229E,
132 suggesting that BST-2 can also restrict viruses that bud in the ERGIC and then are
133 released from the cell via vesicle fusion(37).

134

135 In this study we found that BST-2 restricts SARS-CoV virion egress by
136 tethering virions to the plasma membrane. We also identified several SARS-CoV
137 proteins that are putative modulators of BST-2 function. Focusing on ORF7a, we
138 found that ORF7a directly binds BST-2 and when co-expressed with BST-2, ORF7a

localizes to the plasma membrane, rather than the ER and Golgi. Additionally, we demonstrate that the interaction of ORF7a and BST-2 results in inhibition of BST-2 glycosylation leading to a reduced tethering function in cells and subsequent loss of BST-2 anti-viral function. Together, these data indicate a novel role for SARS-CoV ORF7a as an inhibitor of BST-2, as well as reveal a novel mechanism for altering the function of BST-2.

Materials and Methods

Viruses and cells. icSARS-CoV and icSARS-ORF7abΔ-CoV were constructed as previously described(41, 42). All virus stocks were stored at -80°C until ready to use. Vero E6 cells were purchased from ATCC (catalog number CRL-1586; Manassas, VA) and were grown in minimal essential medium (MEM) (Invitrogen, Carlsbad, CA) with 10% fetal bovine serum (FBS) (Atlanta Biologicals, Lawrenceville, GA), 2mM L-Glutamine (Life Technologies, Grand Island, NY), and 1% penicillin/streptomycin (Gemini Bioproducts, West Sacramento, CA). HEK293T cells were grown in Dulbecco's minimal essential medium (DMEM) (Invitrogen, Carlsbad, CA) with 10% fetal bovine serum (FBS) (Atlanta Biologicals, Lawrenceville, GA), 2mM L-Glutamine (Life Technologies, Grand Island, NY), and 1% penicillin/streptomycin (Gemini Bioproducts, West Sacramento, CA). HEK293T ACE2 cells were a gift from David Wentworth (J Craig Venter Institute) and were grown in HEK293T media supplemented with 1mg/mL G418 (Corning, Manassas, VA).

Plasmids. We received BST-2/Flag in pCAGGS as a gift from Sina Bavari(24). We received ORF7a-Fc as a gift from Andrew Pekosz. The ORF3a, ORF3b, ORF6, ORF7a, ORF8a, S, E, Membrane, N, and PL_{Pro} SARS-CoV plasmids were produced from previous work(6, 7). The nonstructural proteins were cloned into the CAGGS/GFP (green fluorescent protein) or CAGGS/HA (Hemagglutinin) vector for expression in HEK293T cells as previously described(7). Amplicons were produced using the primers shown in **(Table 1)**. For each construct, an ATG start codon was added as the first codon but no stop codon was included at the 3′ terminus of each ORF. Rather, an HA or GFP tag was fused in frame to each ORF. The amplicons and vector were digested with EcoRI/XmaI fragments for cloning, and all constructs were verified by sequence analysis.

SARS-CoV growth curve. HEK293T/hACE2 cells were plated in a 24 well plate and grown overnight at 37°C. Cells were transfected with 2 ul of Lipofectamine LTX (Invitrogen, Carlsbad, CA) and 700 ng of BST-2 Flag in pCAGGS, ORF7a-HA or MISSION pLKO.1-puro non-mammalian shRNA control plasmid (Sigma-Aldrich, St. Louis, MO) according to the manufacturers' instructions. For the glycosylation mutant experiments, pCR3.1-EXN-tetherin-HA(463) and pCR3.1-EXN-tetherin(N65A/N92A)-HA(463) were kindly provided by Dr Paul Bieniasz(29). 24 hours post-transfection, HEK293T ACE2 cells were infected with icSARS-CoV or icSARS-GFP-CoV at a multiplicity of infection (MOI) of 0.1. Supernatant was taken at 12, 24, and 36 hours post-infection to measure SARS-CoV titer by plaque assay on

Vero E6 cells. Supernatant and cell lysate was also analyzed by Western blot. The growth curve experiments were repeated twice with an n of 6 for each sample.

SARS-CoV RNA products of replication were assessed by RT-PCR. RNA from cells infected with SARS-CoV for 24 hours was isolated using Trizol® reagent (Ambion) according to the manufacturers' instructions. RNA was converted to cDNA using RevertAid RT-PCR (Thermo Scientific) according to the manufacturers' instructions and treated with RNase H (New England Biolabs) according to the manufacturers' instructions. Levels of SARS-CoV pp1a (forward primer: GCCGTAGTGTCAGTATCATCACC; reverse primer: AATAGGACCAATCTCTGTAAGAGCC) and N protein mRNA (forward primer: CTCTTGTAGATCTGTTCTCTAAACGAAC; reverse primer: TTACTGTACTAGCAAAGCAATATTGTCG) were quantified using Sybr® green PCR master mix (Applied Biosystems) according to the manufacturers' instructions and a 7500 fast Dx real-time PCR instrument (Applied Biosystems). Levels of SARS-CoV RNA were quantified using the ΔΔCt method. Means and standard deviations were calculated from 3 independent infections.

Electron Microscopy. Vero E6 cells were plated in a 24 well plate and grown overnight at 37°C. Cells were transfected using Lipofectamine LTX (Invitrogen, Carlsbad, CA) with BST-2 Flag in pCAGGS or MISSION pLKO.1-puro non-mammalian shRNA control plasmid (Sigma-Aldrich, St. Louis, MO) according to the manufacturers' instructions. 24 hours post-transfection, Vero cells were infected with icSARS-CoV or icSARS-GFP-CoV at an MOI of 10. At 24 hours post-infection cells

were fixed and analyzed by electron microscopy. For conventional ultrastructural investigations, infected VERO E6 cells were fixed with 2.5% Glutaraldehyde (E.M. Sciences, Warrington, PA) at 24 hours post-infection. After fixation for 72 hours, the preserved cells were post-fixed in 1.0% Osmium Tetroxide (E.M. Sciences), en bloc stained with 2.0% Uranyl Acetate, dehydrated in a series of graded ethanol, and infiltrated and embedded in Spurr plastic resin (Tousimis Research, Rockville, MD). Embedded blocks were sectioned using a Leica UC7 Ultramicrotome, collected thin-sections were mounted on 200 mesh copper grids, contrasted with Lead Citrate, and subsequently viewed at 80 kV with a FEI Tecnai Twin Transmission Electron Microscope. The scale bar shown on Figure 2 is 500nm.

BST-2:SARS-CoV accessory protein co-transfections. HEK293T cells were transfected with 500 ng total DNA using Lipofectamine LTX (Invitrogen, Carlsbad, CA) according to the manufacturers' instructions. 100 ng of BST-2 Flag in pCAGGS, 200 ng or 400 ng of GFP- or HA-tagged SARS-CoV proteins, and MISSION pLKO.1-puro non-mammalian shRNA control plasmid (Sigma-Aldrich, St. Louis, MO) were co-transfected into HEK293T cells. After 18 hours of expression, cells were lysed in lysis buffer (20 mM Tris-HCL [pH 7.6], 150 mM NaCl, 1% NP-40, 0.5% SDS, 5 mM EDTA, 1 protease inhibitor tablet). Lysate was combined with 2X Laemmli Sample Buffer (Bio-Rad, Hercules, CA) before boiling and electrophoresis using Mini-PROTEAN TGX Gels (Bio-Rad, Hercules, CA). Protein expression was assessed using rabbit anti-HA antibody (Sigma-Aldrich, St. Louis, MO), rabbit anti-GFP antibody (Sigma-Aldrich, St. Louis, MO), mouse anti-Flag M2 antibody (Sigma-Aldrich, St.

Louis, MO), and mouse anti-β-tubulin antibody (Sigma-Aldrich, St. Louis, MO). For inhibition experiments cells were transfected as above and four hours post-transfection, media was removed and replaced with 20 nM Concanamycin A (Sigma-Aldrich, St. Louis, MO) or 500 nM MG-132 (Sigma-Aldrich, St. Louis, MO). Cell lysate was collected after 18 hours of drug treatment. For time course experiments HEK-293T were transfected with 500 ng of ORF7a or control plasmid using Lipofectamine LTX (Invitrogen, Carlsbad, CA) according to the manufacturers' instruction. After 6 hours of expression, media was replaced with fresh HEK293T media. 22 hours post-transfection, cells were transfected with 500 ng of DNA, 100 ng of BST-2 plasmid and 400 ng control plasmid, using Lipofectamine LTX (Invitrogen, Carlsbad, CA) according to the manufacturers' instruction. Cell lysate was collected as described above at 4, 8, 12, and 16 hours after the second transfection. Expression was analyzed as described above. Deglyosylation was performed using Glycopeptidase F (Takara, Mountain View, CA) according to the manufacturer's instructions for deglycosylating denatured proteins. The ratio of glycosylated to unglycosylated was calculated by measuring density of the bands with ImageJ (National Institute of Mental Health, Bethesda, MD). All of the transfection experiments were repeated at least two times.

Anti-Flag immunoprecipitations. HEK293T cells were transfected with 1000 ng total DNA using Lipofectamine LTX (Invitrogen, Carlsbad, CA). 500 ng of Flag-tagged BST-2 and 500 ng of SARS PL_{Pro}-GFP, nsp1-GFP, ORF6-GFP, or ORF7a-HA or MISSION pLKO.1-puro non-mammalian shRNA control plasmid (Sigma-Aldrich, St.

Louis, MO) was co-transfected into HEK293T cells. After 18 h of expression, cells were lysed in lysis buffer (20 mM Tris-HCL [pH 7.6], 150 mM NaCl, 1% NP-40, 0.5% SDS, 5 mM EDTA, 1 protease inhibitor tablet), the extract was centrifuged for 10 min at 4°C, and the supernatant was removed. EZ View Red Anti-Flag M2 Affinity Gel beads (catalog number F2426; Sigma, St. Louis, MO) was added to each extract and rotated overnight at 4°C. The extract was then washed twice with lysis buffer and eluted using 0.1 M Glycine (pH 3.5). The elution was combined with 2X Laemmli Sample Buffer (Bio-Rad, Hercules, CA) before boiling and electrophoresis using Mini-PROTEAN TGX Gels (Bio-Rad, Hercules, CA). Protein levels were assessed using rabbit anti-HA antibody (Sigma-Aldrich, St. Louis, MO) and mouse anti-Flag M2 antibody (Sigma-Aldrich, St. Louis, MO). Co-immunoprecipitation experiments were performed twice.

Confocal microscopy. HEK293T cells were seeded onto microscope cover glass (Fisher Scientific, Pittsburg, PA) pre-treated with fibronectin (Sigma-Aldrich, St. Louis, MO) for 30 minutes. HEK293T cells were transfected with 500 ng total DNA using Lipofectamine LTX (Invitrogen, Carlsbad, CA) according to the manufacturers' instructions. 250 ng of BST-2 Flag in pCAGGS, ORF7a-HA, and/or MISSION pLKO.1-puro Non-Mammalian shRNA Control Plasmid (Sigma-Aldrich, St. Louis, MO) were transfected. At 24 hours posttransfection, cells were fixed with 4% formaldehyde overnight at 4°C, then incubated in cold PBS for 10 minutes at room temperature (RT). Each sample was permeabilized with permeabilization buffer (phosphate-buffered saline [PBS], 0.1% Triton X-100, 0.5% bovine serum albumin (BSA)) for 15

minutes at RT and then blocked for 5 minutes using blocking buffer (PBS, 5% BSA). The cells were washed using wash buffer (PBS, 1% BSA, 0.05% NP40) and then stained for protein expression. Primary antibodies used were rabbit anti-HA antibody (Sigma-Aldrich, St. Louis, MO) and mouse anti-Flag M2 antibody (Sigma-Aldrich, St. Louis, MO). Cells were incubated with primary antibodies diluted in antibody dilution buffer (PBS, 1% BSA, 0.05% NP40, 2% normal goat serum) for 45 minutes at RT. Cells were washed three times with wash buffer and then incubated while rocking for 30 minutes at room temperature with goat anti-rabbit IgG conjugated with AMCA (Vector Laboratories, Burlingame, CA) and/or horse anti-mouse conjugated with Texas Red (Vector Laboratories, Burlingame, CA). Cells were then washed with wash buffer 3 times and a final time with PBS for 30 minutes at RT. For the ORF7a localization experiments the endoplasmic reticulum (ER) was stained with Concanavalin A, Alexa Fluor® 594 Conjugate (Invitrogen, Carlsbad, CA) and the Golgi was stained with BODIPY TR Ceramide complexed to BSA (Invitrogen, Carlsbad, CA) according to the manufacturer's instructions. The coverslips were then mounted on slides using VECTASHIELD Hard Set Mounting Medium with DAPI (Vector Laboratories, Burlingame, CA). Slides were analyzed by confocal microscopy using a Zeiss LSM 510 microscope. Images were collated and adjusted using ImageJ (National Institute of Mental Health, Bethesda, MD).

Flow Cytometry.

For experiments to determine BST-2 surface expression, HEK293T cells were transfected as above with BST-2 and ORF7a. After 18 hours of expression cells were washed with PBS and dissociated with 0.05% Trypsin-EDTA (1X), phenol red (Invitrogen, Carlsbad, CA). Cells were washed in HEK293T media to inactivate the Trypsin and were resuspended in FACS buffer (PBS with 1% fetal bovine serum) and stained for 20 minutes with APC anti-human CD317 Clone RS38E (Biolegend, San Diego, CA) or control Mouse IgG_1 APC (Becton Dickinson, Franklin Lakes, NJ). Cells were then washed, resuspended in FACS buffer, and analyzed on a LSRII flow cytometer (Becton Dickinson, Franklin Lakes, NJ). Data was analyzed using Flowjo (Tree Star, Ashland, OR).

For experiments to determine mutant BST-2 surface expression, 293T cells were plated 250,000 per well in 6-well plates, grown overnight at 37^0C with 5% CO_2 and then transfected with 1 ug of each DNA (empty vector, empty vector + WT BST2, empty vector + mt BST2, empty vector + ORF 7a, WT BST2 + ORF 7a, mt BST2 + ORF 7a). All following steps were performed at room temperature. At twenty-four hours after transfection, cells were harvested using Cell Dissociation Buffer (Invitrogen). Duplicate transfected wells were pooled and samples transferred to a 96-well plate. Cells were pelleted at 2000 rpm for 2 minutes, fixed in 4% paraformaldehyde for 5 minutes, then washed with 10%FBS/PBS and pelleted as above. Samples were divided into 2 aliquots then blocked with 10%FBS/PBS, or blocked/permeabilized with 10% saponin in 10%FBS/PBS for 30 minutes. Cells were pelleted as above and incubated in primary antibodies for 1 hour (HA antibody, Sigma H6908 and FLAG antibody, Sigma F3165, 1:1000). Cells were washed 2 times with 10%FBS/PBS and

pelleted as above. Secondary antibodies (FITC anti-rabbit, Vector Labs and Alexa 405 anti-mouse, ThermoFisher, 1:1000) were added to cells and incubation was 1 hour, followed by washing and pelleting as above. Cells were resuspended in PBS and cell surface localization as well as total cell expression of BST2 and ORF 7a were determined using an LSRII flow cytometer. Control (no DNA), BST2 or ORF 7a transfected alone were used as compensation controls. Data was analyzed using FlowJo and statistical analysis was generated from a t test generated using standard errors based on results from three individual experiments.

Circular Dichroism (CD) of BST2 and ORF7a-Fc.

CD spectra ranging from 200-260nm were recorded in 10mM Sodium phosphate buffer pH7.5 of 10μM BST2 expressed in HEK293T cells, 12μM BST2 expressed in *E.coli* cells and 8μM ORF7a-Fc expressed in HEK239T cells using a JASCO J-810 instrument. CD melting curves were analyzed at 222nm by increasing the temperature 1°C/min starting at 20°C.

Surface Plasmon Resonance. 21 μg of pCAGGS-T7/ORF7a-Fc was transfected into HEK293T cells seeded in 100 mm dishes using Lipofectamine LTX (Invitrogen, Carlsbad, CA) according to the manufacturers' instructions. After 48 hours of expression, supernatant was collected and purified using a HiTrap Protein A column (GE Healthcare, Little Chalfont, Buckinghamshire, UK) according to the manufacturer's instructions. Purified ORF7a-Fc was subsequently dialyzed into PBS. The codon-optimized sequence of the extracellular domain (residues 47-161) of

344 BST-2 was cloned with a N-terminal His_6- and a C-terminal Flag-tag into pET28b.
345 The protein was expressed at 19°C overnight in BL21(DE3)pLysS cells induced at an
346 OD_{600} of 0.6 with 0.4mM IPTG. The fusion protein was purified by nickel affinity
347 (Thermo Scientific, Pittsburg, PA), using a Mono Q™ 5/50GL anion exchange column
348 (GE Healthcare, Little Chalfont, Buckinghamshire, UK) and finally separated on a
349 Superdex™ 200 10/300 GL gel filtration column (GE Healthcare, Little Chalfont,
350 Buckinghamshire, UK). The extracellular domain (residues 47-161) of BST-2 was
351 also cloned into the plGplus Vector (R&D Systems, Minneapolis, MN). The resulting
352 BST-2 protein includes a C-terminal His_6-Flag-tag and due to the encoded stop
353 codon did not express as an Fc fusion protein. HEK293T cells in suspension culture
354 were transfected with this construct using polyethylenimine (Polysciences, Inc.,
355 Warrington, PA). The cell culture supernatant was harvested 96 hours post-
356 transfection and purified using nickel affinity (Thermo Scientific, Pittsburg, PA)
357 followed by gel filtration on a Superdex™ 200 10/300 GL column (GE Healthcare,
358 Little Chalfont, Buckinghamshire, UK). Direct binding of the extracellular domain of
359 ORF7a-Fc expressed in HEK293T cells to the extracellular domain of BST-2
360 expressed in *E. coli* or HEK293T cells was measured by surface plasmon resonance
361 (SPR) analysis using a Biacore T100 instrument (GE Healthcare, Little Chalfont,
362 Buckinghamshire, UK). 1000 RU of protein A was immobilized by amine coupling on
363 the surface of a CM5 sensor chip. Approximately 170 RU of human IgG (Sigma-
364 Aldrich, St. Louis, MO) as negative control and also of ORF7a-Fc was captured on
365 flow cells 1 and 2, respectively. In single-cycle kinetics experiments, two-fold
366 dilutions from 80 to 5 µM of BST-2 were injected over the surfaces and the control-

subtracted response was recorded. HBS-EP was used as a running buffer and the surfaces were regenerated with 20 mM HCl after each cycle. Steady-state analysis of the data was performed using the Biacore T100 Evaluation Software 2.0.3. All of the SPR experiments were repeated at least three times.

Statistical analysis. Growth curve titers were analyzed by t-test using the Holm_Sidak method with alpha=5.0%. Prism (GraphPad Software Inc., La Jolla, CA) was used to perform the analysis.

Results

SARS-CoV proteins antagonize BST-2 expression *in vitro*. Many enveloped viruses, including the coronavirus hCoV-229E, encode proteins that counteract BST-2 (24, 27, 37). We hypothesized that the highly pathogenic SARS-CoV may also inhibit BST-2 function. To investigate this hypothesis, HA- and GFP-tagged SARS-CoV proteins and BST-2 were co-transfected into HEK293T cells and BST-2 expression levels were assessed by Western blot. Four SARS-CoV proteins, non-structural protein 1 (nsp1), the papain-like protease domain of nsp3 (PL_{Pro}), ORF6, and ORF7a altered BST-2 protein expression or molecular weight. Several proteins encoded in the SARS-CoV genome have been shown to alter other anti-viral response pathways during infection(43-53). Three of the proteins, papain-like protease (PL_{Pro}), ORF6, and nsp1, have been previously shown to be interferon antagonists(7, 8, 54). PL_{Pro} inhibits IRF3 and NFkB activation(54), ORF6 blocks

STAT1 nuclear import, and nsp1 blocks interferon beta induction by degrading host mRNAs(6, 7, 54, 55). Because the function of ORF7a is unclear, we decided to further study interactions between BST-2 and ORF7a.

icSARS-ORF7abΔ-CoV shows defects in replication compared to icSARS-CoV when BST-2 is overexpressed. Since ORF7a affects BST-2 protein, we hypothesized that an ORF7ab deletion SARS-CoV (icSARS-ORF7abΔ-CoV) would show a greater defect in replication compared to WT SARS-CoV when BST-2 is overexpressed. Since ORF7a and ORF7b have overlapping open reading frames, an ORF7ab double deletion virus will be used for the infection experiments. No effect on BST-2 was found when ORF7b was expressed alone in the assays in transfection screens. We transfected HEK293T/hACE2 cells with BST-2 or a control plasmid and 24 hours post-transfection we infected the cells with either icSARS-CoV or icSARS-ORF7abΔ-CoV at an MOI of 0.1. HEK293T cells do not express endogenous BST-2(27), so we were able to ensure that any effect was from the transfected BST-2 and not endogenous BST-2 expression. icSARS-CoV replicated to 1.10×10^5 PFU/mL, while in BST-2 expressing cells icSARS-CoV replicated to significantly lower titers at 3.43×10^4 PFU/mL (Figure 1a, $p<0.01$). icSARS-ORF7abΔ-CoV was also significantly restricted by BST-2 expression at 24 and 36 hours. In control transfected cells icSARS-ORF7abΔ-CoV replicated to 7.37×10^4 PFU/mL and 4.80×10^4 PFU/mL at 24 and 36 hours respectively, while in BST-2 transfected cells icSARS-ORF7abΔ-CoV replicated to significantly lower titers of 4.00×10^3 PFU/mL ($p<0.05$) and 1.10×10^4 PFU/mL ($p<0.001$) at 24 and 36 hours, respectively (Figure

1b). While BST-2 restricts SARS-CoV by a small, but significant amount, BST-2 restricts icSARS-ORF7abΔ-CoV by a much greater amount, suggesting that ORF7a antagonizes BST-2.

We confirmed that BST-2 is not affecting another step in the SARS-CoV replication cycle by assessing the accumulation of SARS-CoV RNA products of replication in the presence of BST-2 at 24 hours post infection. There is no significant effect of BST-2 expression on SARS-CoV pp1a (Figure 1c) or SARS-CoV N mRNA (Figure 1d), regardless of ORF7a expression. These data suggest that BST-2 does not effect SARS-CoV RNA accumulation, even in the absence of ORF7a expression.

icSARS-ORF7abΔ-CoV defect in replication is due to direct tethering of SARS-CoV virions to the plasma membrane. Since BST-2 has been shown to restrict virus replication by directly tethering HIV-1 virions to the plasma membrane(27, 56), we sought to determine if overexpression of BST-2 was preventing release of SARS-CoV and if icSARS-ORF7abΔ-CoV was more susceptible to BST-2 restriction. To determine if BST-2 was affecting release, we transfected either BST-2 or a control plasmid into VeroE6 cells and subsequently infected with either icSARS-CoV or icSARS-ORF7abΔ-CoV at a MOI of 10. At 24 hours post-infection cells were fixed and imaged using electron microscopy. When VeroE6 cells were transfected with the control plasmid, both icSARS-CoV and icSARS-ORF7abΔ-CoV showed minimal accumulation of virions at the plasma membrane (Figure 2). Transfection of BST-2 leads to a small accumulation of icSARS-CoV on plasma membrane (Figure 2, top

left). BST-2 transfection shows a much greater effect on icSARS-ORF7abΔ-CoV, which shows a large accumulation of virions at the plasma membrane (Figure 2, top right). These results confirm that similar to many other viruses, BST-2 is restricting SARS-CoV by preventing virus release. The increased effect of BST-2 on icSARS-ORF7abΔ-CoV further suggests that ORF7a acts as an inhibitor BST-2-mediated restriction of SARS-CoV.

ORF7a expression leads to lower molecular weight BST-2 within the cells, but not reduced BST-2 surface expression. Since ORF7a appears to be a BST-2 antagonist, we aimed to determine if SARS-CoV ORF7a causes BST-2 surface removal and subsequent degradation, as seen in HIV-1 Vpu protein antagonism(33, 56). SARS-CoV ORF7a was co-transfected with increasing amounts of BST-2 to assay the effect of ORF7a on BST-2 expression. Increasing the amount of ORF7a co-transfected with BST-2 leads to decreased levels of BST-2 expression and lower molecular weight products, suggesting that BST-2 protein is affected by ORF7a expression (Figure 3a). Next, we sought to determine if, similarly to HIV-1 Vpu, expression of ORF7a leads to a reduction in BST-2 surface expression(56). To assay the effect of ORF7a on BST-2 surface expression, we transfected BST-2 either alone or in combination with an ORF7a expression plasmid to compare BST-2 surface expression by flow cytometry. Untransfected cells exhibited little to no expression of surface BST-2. Cells transfected with BST-2 alone were 88.2% positive with the majority of cells in a highly expressing population and a smaller percentage in a lower expressing population (Figure 3b). Interestingly, increasing amounts of

ORF7a had no effect on surface expression of BST-2 (Figure 3b). These data demonstrate that ORF7a co-expression leads to lower molecular weight BST-2 within cells, but does not lead to surface removal of BST-2, suggesting that ORF7a may antagonize BST-2 through a mechanism other than surface removal.

Lysosomal and proteasomal inhibitors do not affect BST-2 antagonism by ORF7a. While we did not observe ORF7a dependent removal of surface BST-2, we did observe the appearance of lower molecular weight bands of BST-2, suggesting degradation of intracellular BST-2. Many other viruses, such as HIV-1, antagonize BST-2 by degradation through either the lysosome or proteasome and, thus, we assessed whether lysosomal or proteasomal inhibitors could block BST-2 antagonism by ORF7a(32-34). First, to demonstrate that the concentration of Concanamycin A (Con A) and MG-132 inhibit proteasome and lysosomal degradation, respectively, in HEK293T cells, we treated cells and assayed for Ubiquitin and LC3B levels by western blot (Figure 4A and B). As expected, MG-132 treatment increases total ubiquitin levels in the cell (Figure 4A) and Con-A treatment blocks lysosomal degradation, as shown with an increase in the lower weight LC3B product. To test for the effect of proteosomal or lysosomal effects on BST-2 antagonism, we transfected HEK293T cells with BST-2 and ORF7a or a control plasmid and at four hours post-transfection, replaced the media with media containing either 20 nM Concanamycin A (to inhibit lysosomal degradation) or 500 nM MG-132 (to inhibit proteasome function). At 18 hours post-transfection, cells were lysed and analyzed by Western blot to determine if BST-2 was degraded. After

Journal of Virology

treatment, lower molecular weight bands were still observed. Treatment with neither Concanamycin A nor MG-132 blocked the ability of ORF7a to antagonize BST-2 (Figure 4C). The far right 2 lanes contain a background band at a similar molecular weight as HA-tagged ORF7a that does not affect the experiment. These data demonstrate that the appearance of lower molecular weight bands of BST-2 is not due to lysosomal or proteasomal degradation and suggests that ORF7a antagonizes BST-2 through an alternative mechanism.

BST-2 colocalizes with and alters localization of SARS-CoV ORF7.. Since icSARS-ORF7abΔ-CoV is more susceptible to BST-2 restriction and ORF7a appears to cause the appearance of a low molecular weight BST-2 band, we hypothesized that BST-2 may alter ORF7a localization within the cell. ORF7a was transfected into HEK293T cells and the cells were stained for ORF7a, as well as ER and Golgi markers(9, 10). ORF7a normally localizes to the Golgi and was also detectable in the ER, as would be expected for a protein that passes through the ER to the Golgi (Figure 5a). To determine if BST-2 and ORF7a co-localize, we performed confocal microscopy. When transfected alone, ORF7a localizes primarily to the Golgi, whereas BST-2 localizes to the plasma membrane (Figure 5b). When BST-2 and ORF7a were co-transfected, ORF7a now appears to localize to the plasma membrane, coincident with BST-2 (Figure 5b). These data suggest that BST-2 and ORF7a may be interacting in cells.

SARS-CoV ORF7a co-immunoprecipitates with BST-2. Having shown that ORF7a both alters protein mobility and localizes to the plasma membrane when co-expressed with BST-2, we sought to determine if there is a molecular interaction between the two proteins. We co-transfected BST-2 and ORF7a into HEK293T cells and 18 hours post-transfection cells were lysed. We immunoprecipitated proteins from transfected cells and immunoblotted for both BST-2 and ORF7a. We found BST-2 and ORF7a present in both the input and the co-immunoprecipitation (Figure 6) suggesting an interaction between BST-2 and ORF7a, either directly or within a larger multi-component complex.

Direct interaction between ORF7a and BST-2 is regulated by BST-2 glycosylation. To assess whether the extracellular domain of ORF7a interacts directly with the extracellular domain of BST-2, we performed surface plasmon resonance (SPR) analysis of ORF7a-BST-2 binding. SPR allows direct quantitation of protein-protein interaction by measuring the affinity between two proteins. One protein is immobilized on a sensor chip and the other is flowed over the sensor chip in increasing concentrations. Binding of proteins causes changes in refraction, which is detected and recorded as resonance units (RU). Affinity can then be calculated from changes in RU(57). ORF7a with an Fc fusion tag (ORF7a-Fc) was expressed and purified from HEK293T cells and BST-2 was expressed and purified from both *E. coli* and HEK293T cells (Figure 7A). CD spectra of BST2 expressed in HEK239T and *E.coli* cells both reveal the expected pattern for a protein containing primarily α–helical folds (Figure 7B). ORF7a-Fc, in contrast, shows the typical spectrum of

proteins formed dominantly by β–sheets (Figure 7B). Melting temperatures were deduced from the melting curves (Figure 7C) and tetrameric BST2 expressed in *E.coli* cells has a slightly lower melting temperature of 61.95°C than dimeric BST2 expressed in HEK293T cells, 65.3°C (Figure 7C). These data suggests that both BST-2 and ORF-7a-Fc are folded correctly and were, therefore, used for the SPR analysis.

By SPR, we observed that unglycosylated BST-2 expressed in *E. coli* was able to bind to ORF7a-Fc with an affinity (K_D) of 10 μM (Figure 7D). Binding of glycosylated BST-2 expressed in HEK293T cells, though, exhibited markedly weaker responses in identical SPR experiments, which did not reach equilibrium and, therefore, did not allow us to quantify an accurate K_D for this interaction (Figure 7E). We did attempt to fit the data to estimate the K_D for this interaction and the binding of ORF7a to glycosylated BST-2 is at least 4 times weaker than to unglycosylated BST-2. These data indicate that ORF7a binds directly to unglycosylated BST-2 with μM affinity and that the presence of *N*-linked glycosylation at positions 65 and 92 of BST-2 significantly weakens this interaction.

ORF7a expression interferes with BST-2 glycosylation. Given that ORF7a-dependent BST-2 antagonism is unaffected by lysosomal or proteasomal inhibitors and that ORF7a binds unglycosylated BST-2 with substantially higher affinity than glycosylated BST-2, we hypothesized that ORF7a may bind to BST-2 before it is glycosylated in the ER and interfere with glycosylation of BST-2. To determine if ORF7a interferes with glycosylation, we transfected HEK293T cells with increasing amounts of ORF7a. Co-transfection of increasing amounts of ORF7a leads to lower

molecular weight bands of BST-2 in a dose-dependent manner (Figure 8). To confirm that the lower molecular weight bands were unglycosylated, we treated lysate from cells expressing BST-2 with glycopeptidase F. Previous studies have shown that treatment with glycopeptidase F removes all the glycosylation from BST-2(30). The BST-2 lysate treated with glycopeptidase F showed a shift to a lower molecular weight with an identical size as the lower molecular weight band present when BST-2 is co-transfected with ORF7a (Figure 8a). To further confirm that co-transfection of ORF7a leads to decreased levels of unglycosylated BST-2, we measured the density of each band and calculated the ratio of glycosylated to unglycosylated BST-2. As the levels of ORF7a increase, the levels of glycosylated BST-2 decrease (Figure 8b). These data suggests that ORF7a interferes with glycosylation of BST-2.

Unglycosylated BST-2 no longer restricts icSARS-ORF7abΔ-CoV release.

To confirm that glycosylation of BST-2 is necessary for restriction of icSARS-ORF7abΔ-CoV, we transfected 293T/ACE2 cells with a mutant of BST-2 that does not undergo *N*-linked glycosylation (called N65A/N92A) (29). We confirmed expression of the N65A/N92A mutant BST-2 by western blot, where we observed only expression of the expected 19kDa unglycosylated form of BST-2 (Figure 9A). We then confirmed that the N65A/N92A mutant was still able to localize to the cell surface by quantifying the amount of WT and mutant BST-2 by flow cytometry on non-permeabilized cells. Surface labeling shows that mutant BST-2 localization to the plasma membrane is not significantly different from WT BST-2 surface

expression (Figure 9B). We transfected cells with plasmids encoding WT and N65A/N92A mutant BST-2 and then infected those cells with WT icSARS-Urbani or icSARS-ORF7ab Δ -CoV. The BST-2 plasmid used in these experiments has a HA tag inserted at amino acid 463, so we first confirmed that HA/BST-2 is still able to significantly (10-fold, p =.0046) restrict icSARS-ORF7abΔ-CoV compared to icSARS-Urbani (Figure 9C). However, there was no significant difference between supernatant icSARS-Urbani and icSARS-ORF7abΔ-CoV in cells transfected with N65A/N92A mutant BST-2 (Figure 9C, p =0.274), suggesting that *N*-linked glycosylation is required for the BST-2 mediated restriction of icSARS-ORF7abΔ-CoV.

Discussion

Our studies further expand the role of BST-2 in restriction of enveloped viruses. We screened selected genes from the SARS-CoV genome and identified four potential BST-2 modulators, of which one was SARS-CoV ORF7a. While ORF7a has been shown to induce apoptosis, a definitive role has not been established for ORF7a during infection(13-15). Through overexpression, infection and transfection studies we demonstrate that BST-2 blocks the release of SARS-CoV virions, that ORF7a overcomes this inhibition and that ORF7ab deleted viruses display increased sensitivity to BST-2. Importantly, the inhibition of BST-2 is not by protein degradation, but by inhibiting its activity through inhibiting glycosylation at two key sites on the protein that are required for its anti-viral function. We demonstrate that a BST-2 mutant protein with the two glycosylation sites removed, still traffics to the plasma membrane, but is unable to inhibit SARS-CoV release. Our data also

demonstrate that, unlike HIV-1 Vpu, which removes BST-2 protein from the surface and induces degradation(32, 33, 56), SARS-CoV ORF7a does not remove BST-2 from the plasma membrane

We have confirmed the interaction of ORF7a and BST-2 using multiple assays including immunoprecipitation, co-localization and surface plasmon resonance, which show that ORF7a directly binds to unglycosylated BST-2, but not glycosylated BST-2. Previous studies have suggested that glycosylation of BST-2 is required for BST-2 anti-viral activity(29) and the amino acid residues surrounding the *N*-linked glycosylation sites are evolutionarily conserved in BST-2 suggesting that these amino acids may be important for BST-2 function(22). We further demonstrated that *N*-linked glycosylation is required for the restriction of SARS-CoV lacking ORF7a, suggesting that the blocking of glycosylation by ORF7a is directly responsible for the antagonism of BST-2. BST-2 *N*-linked glycosylation has been proposed to effect the HIV-1 restriction activity of BST-2(27, 29, 33, 56, 58), however, we have demonstrated for the first time that a virus encodes a BST-2 antagonist that inhibits BST-2 glycosylation, providing a potential mechanism for other viral putative BST-2 antagonists.

Taken together, the data suggests that ORF7a may function by binding to and preventing *N*-linked glycosylation of BST-2, preventing the tethering of SARS-CoV virions to the cytoplasmic membrane after they are released from the cell. We hypothesize that while BST-2 is trafficking through the ER and Golgi to the surface,

Journal of Virology

619 ORF7a and BST-2 interact in the Golgi, where the extracellular domain of ORF7a
620 binds the unglycosylated extracellular domain of BST-2 and either directly prevents
621 glycosylation of BST-2 or binds to the evolutionarily conserved sites and as a side-
622 effect blocks *N*-linked glycosylation. SARS-CoV virions form in the ERGIC during
623 virion maturation and it is yet to be determined if ORF7a or BST-2 are present in
624 those compartments. Potentially BST-2 is binding newly released SARS-CoV
625 virions at the plasma membrane, however, most models of BST-2 function predict
626 that BST-2 is inserted into the membrane the virion as it forms(20), so we would
627 predict that BST-2 will first interact with SARS-CoV virions in the ERGIC.
628
629 While a variety of enveloped viruses encode BST-2 antagonists, those antagonists
630 function by different mechanisms. HIV-1 Vpu and Kaposi-Sarcoma Herpesvirus K5
631 both ubiquitinate BST-2, leading to surface removal and subsequent lysosomal
632 degradation(27, 56, 59). HIV-2 Env also removes BST-2 from the surface, but rather
633 than being degraded, BST-2 is relocated to the trans-Golgi network and cannot
634 function as a cytoplasmic membrane tether(36). SIV Env removes BST-2 from the
635 surface through BST-2 internalization by endocytosis(38, 60). Ebolavirus GP1,2
636 does not remove BST-2 from the surface, but antagonizes BST-2 through an as yet
637 unknown mechanism(39). The diverse mechanisms of known BST-2 antagonists
638 demonstrate that viruses have independently evolved many different ways of
639 antagonizing BST-2, an important restriction factor for any enveloped virus. It is
640 possible that all enveloped viruses encode, in most cases undiscovered, BST-2
641 antagonists that act by a variety of mechanisms.

In this study we have identified BST-2 as a potential inhibitor of SARS-CoV release. Our studies suggest that SARS-CoV ORF7a antagonizes the function of BST-2 by interfering with its *N*-linked glycosylation while binding it in the Golgi and then trafficking with it from the Golgi to the plasma membrane. From this we predict that therapeutics designed to inhibit the interaction between BST-2 and ORF7a may inhibit virus growth *in vitro* and *in vivo*.

Acknowledgements

This work was supported by the Division of Intramural Research of the National Institute of Allergy and Infectious Diseases (NIAID) with grant RO1AI1095569 (MBF) and by NIAID grant R01AI087452 (EJS).

665

SARS-CoV Gene	Forward Primer/EcoR1 Site
nsp1	5'-GATCGAATTCACCATGGAGAGCCTTGTTCTTGGTGTCA-3'
nsp4	5'-GATCGAATTCACCATGAAGATTGTTAGTACTTGTTTTA-3'
nsp5	5'-GATCGAATTCACCATGAGTGGTTTTAGGAAAATGGCAT-3'
nsp6	5'-GATCGAATTCACCATGGGTAAGTTCAAGAAAATTGTTA-3'
nsp7	5'-GATCGAATTCACCATGTCTAAAATGTCTGACGTAAAGT-3'
nsp8	5'-GATCGAATTCACCATGGCTATTGCTTCAGAATTTAGTT-3'
nsp9	5'-GATCGAATTCACCATGAATAATGAACTGAGTCCAGTAG-3'
nsp10	5'-GATCGAATTCACCATGGCTGGAAATGCTACAGAAGTAC-3'
nsp13	5'-GATCGAATTCACCATGAGGCTGTAGGTGCTTGTGTATTGT-3'
nsp14	5'-GATCGAATTCACCATGGCAGAAAATGTAACTGGACTTTTT-3'
nsp15	5'-GATCGAATTCACCATGAGTTTAGAAAATGTGGCTTATAAT-3'
nsp16	5'-GATCGAATTCACCATGGCAAGTCAAGCGTGGCAACCAG-3'

SARS-CoV Gene	Reverse Primer/XmaI Site
nsp1	5'-GATCCCCGGGACCTCCATTGAGCTCACGAGTGAGT-3'
nsp4	5'-GATCCCCGGGCTGCAGAACAGCAGAAGTGATTGAT-3'
nsp5	5'-GATCCCCGGGTTGGAAGGTAACACCAGAGCATTGT-3'
nsp6	5'-GATCCCCGGGCTGTACAGTAGCAACCTTGATACAT-3'
nsp7	5'-GATCCCCGGGCTGAAGAGTAGCACGGTTATCGAGC-3'
nsp8	5'-GATCCCCGGGCTGTAGTTTAACAGCTGAGTTGGCT-3'
nsp9	5'-GATCCCCGGGCTGAAGACGTACTGTAGCAGCTAAA-3'
nsp10	5'-GATCCCCGGGCTGCATCAAGGGTTCGCGGAGTTGG-3'
nsp13	5'-GATCCCCGGGTTGTAATGTAGCCACATTGCGACGTGGTAT-3'
nsp14	5'-GATCCCCGGGCTGTAACCTGGTAAATGTATTCCACAGGTT-3'
nsp15	5'-GATCCCCGGGTTGTAGTTTTGGGTAGAAGGTTTCAACATG-3'
nsp16	5'-GATCCCCGGGGTTGTTAACAAGAATATCACTTGAA-3'

666

667 **Table 1: SARS-CoV non-structural protein cloning primers.** Cloning primers

668 used in this study

669

670

671

672

673

Journal of Virology

674 **Figure Legends**

675

676 **Figure 1: icSARS-CoV and icSARS-ORF7abΔ-CoV infection of cells with and**
677 **without BST-2 expression.** (A and B) HEK293T ACE2 cells were transfected with
678 BST-2 Flag in pCAGGS or a control plasmid. 24 hours post-transfection, HEK293T
679 ACE2 cells were infected with icSARS-CoV (A) or icSARS-ORF7abΔ-CoV (B) at an
680 MOI of 0.1. Supernatant and cell lysate was taken at 12, 24, and 36 hours post-
681 infection. Virus was titered from supernatant taken at 12, 24, and 36 hours. (B) RNA
682 extracted from icSARS and icSARS-ORF7abΔ-CoV infected HEK293T ACE2 cells was
683 analyzed by realtime PCR for genomic RNA levels (C) or leader containing N mRNA
684 (D) as a signature of replicating virus. * significant at $p < 0.05$, ** significant at $P < 0.01$, *** significant at $P < 0.001$. Data shown is representative of two independent
686 experiments.

687

688 **Figure 2: BST-2 tethers SARS-CoV to plasma membrane**
689 BST-2 or control plasmid was transfected into VeroE6 cells and infected with either
690 icSARS-CoV or icSARS-ORF7abΔ-CoV at an MOI of 10. At 24 hours post-infection
691 cells were fixed and imaged by electron microscopy. Transfection of BST-2 results in
692 a large increase in icSARS-ORF7abΔ-CoV virions retained at the surface compared to
693 control transfected cells. Scale bars equal 500nm.

694

695 **Figure 3: ORF7a expression leads to lower molecular weight BST-2 within the**
696 **cells, but not reduced BST-2 surface expression.**

BST-2 was transfected into HEK293T cells with increasing amounts of ORF7a. 18 hours post-transfection cells were either lysed and analyzed by western blot or stained with an anti-BST-2 antibody conjugated to APC and analyzed using flow cytometry. Untransfected cells did not express BST-2. BST-2 transfected cells showed high BST-2 expression and co-transfection of ORF7a and BST-2 lead to decreased levels of the high molecular weight BST-2 band and increasing levels of a lower molecular weight BST-2 band in a dose-dependent manner (A), but did not lead to reduced surface expression of BST-2 (B). Data shown is representative of two independent experiments.

Figure 4: Proteasomal and Lysosomal inhibitors effect on ORF7a antagonism of BST-2. (A and B) HEK293T cells were treated with either Concanamycin A (ConA) or MG-132 to demonstrate the concentrations used are inhibitory or proteasome or lysosomal degradation, respectively. Lysate was analyzed by western blot for with antibodies against Ubiquitin (A) and LC3B (B) to demonstrate efficacy of compounds. (C) Increasing amounts of ORF7a was transfected into HEK293T cells. Cells were subsequently treated with the lysosome inhibitor, Concanamycin A, or proteasome inhibitor, MG132. Neither inhibitor prevented BST-2 antagonism by ORF7a. Data shown is representative of three independent experiments.

Figure 5: ORF7a Co-localizes with BST-2. HEK293T cells were transfected with BST-2, ORF7a, or both. (A) BST-2 was stained with mouse anti-Flag primary and

goat anti-mouse Texas Red secondary. ORF7a was stained with rabbit anti-HA primary and horse anti-rabbit AMCA secondary. Localization was analyzed with confocal microscopy (merged images shown as yellow). (B) When BST-2 and ORF7a are co-transfected, the two proteins display overlapping signal as seen in the merged image (shown as yellow).

Figure 6: ORF7a Co-Immunoprecipiates with BST-2. HEK293T cells were transfected with sham, ORF7a/HA and BST-2/Flag separately or together. After expressing for 18 hours, cells were lysed and analyzed by western blot for expression (A). BST-2 was immunoprecipitated with anti-Flag beads. Bound protein was eluted and analyzed by Western Blot (B). BST-2 was detected with a mouse anti-Flag M2 antibody. ORF7a was detected with rabbit anti-HA antibodies. ORF7a was detected in the elution from the co-immunoprecipitation suggesting an interaction between ORF7a and BST-2. Data shown is representative of two independent experiments. Asterisk denotes a non-specific band.

Figure 7: Binding of ORF7a to BST-2. (A) Purified BST-2 expressed in *E. coli* and HEK293T cells was stained with Coomassie. BST-2 expressed in *E. coli* has a lower molecular weight than BST-2 expressed in HEK293T cells due to lack of glycosylation. (B) CD spectra and melting curves (C) of BST2 and ORF7a-Fc. CD spectra of 10μM BST2 expressed in HEK293T cells, 12μM BST2 expressed in *E.coli* cells and 8μM ORF7a-Fc expressed in HEK239T cells. (D) Shown are representative sensograms obtained in SPR experiments analyzing direct interaction of ORF7a-Fc

with unglycosylated BST-2 expressed in *E. coli* (D) and glycosylated BST-2 expressed in HEK293T cells (E). For SPR experiments, ORF7a-Fc was captured via immobilized protein A on a CM5 chip. Single-cycle kinetics were performed by injection of 5μM, 10μM, 20μM, 40μM and 80μM of BST-2. Data shown is representative of three independent experiments.

Figure 8: ORF7a interferes with glycosylation of BST-2

BST-2 was transfected into HEK293T cells with increasing amounts of ORF7a. 18 hours post-transfection cells were lysed and analyzed by western blot. (A) Increasing levels ORF7a lead to increased levels of a lower molecular weight band of BST-2, which we hypothesized to be unglycosylated BST-2. To confirm that the lower molecular weight band was unglycosylated BST-2, we treated lysate from BST-2 transfected cells with Glycopeptidase F, which deglycosylates proteins. When treated with Glycopeptidase F, BST-2 shifts down to the same molecular weight as the lower band of BST-2 co-transfected with ORF7 suggesting ORF7a leads to increased levels of unglycosylated BST-2. (B) Density of each band was measured and the ratio of glycosylated to unglycosylated BST-2 was calculated and graphed. Data shown is representative of three independent experiments.

Figure 9: Unglycosylated BST-2 fails to inhibit SARS-CoV egress.

HEK293T/ACE2 cells were transfected with either control plasmid, wildtype HA-tagged BST-2 or a mutant HA-tagged BST-2 containing N65A and N92A mutations. (A) Expression levels of wildtype BST-2 and N65A/N92A BST-2 were analyzed by

western blot with anti-HA antibody and anti-Tubulin as a loading control. N65A/N92A BST-2 runs noticeably slower due to its loss of glycosylation. (B) HEK293T/ACE2 cells were transfected with each plasmid and levels of BST-2 protein on the surface of cells was analyzed by flow cytometry with an anti-HA antibody. The percent of surface expression of BST-2(WT) transfected cells is graphed displaying surface localization of the B65A/N92A mutant BST-2 (C) HEK293T/ACE2 cells were transfected with each plasmid and infected with either icSARS-CoV or icSARS-ORF7abΔ-CoV. Cell supernatants were analyzed by plaque assay and graphed as the % of wildtype icSARS-CoV released. Notice the loss of inhibition of icSARS-ORF7abΔ-CoV release in the mutant BST-2 transfected cells compared to wildtype BST-2 transfected cells. *** equals a P value <0.005

References

1. **Organization WH.** 2003. WHO | Summary of probable SARS cases with onset of illness from 1 November 2002 to 31 July 2003 WHO.
2. **Drosten C, Preiser W, Günther S, Schmitz H, Doerr HW.** 2003. Severe acute respiratory syndrome: identification of the etiological agent. Trends in molecular medicine **9:**325-327.
3. **Marra MA, Jones SJM, Astell CR, Holt RA, Brooks-Wilson A, Butterfield YSN, Khattra J, Asano JK, Barber SA, Chan SY, Cloutier A, Coughlin SM, Freeman D, Girn N, Griffith OL, Leach SR, Mayo M, McDonald H, Montgomery SB, Pandoh PK, Petrescu AS, Robertson AG, Schein JE, Siddiqui A, Smailus DE, Stott JM, Yang GS, Plummer F, Andonov A, Artsob H, Bastien N, Bernard K, Booth TF, Bowness D, Czub M, Drebot M, Fernando L, Flick R, Garbutt M, Gray M, Grolla A, Jones S, Feldmann H, Meyers A, Kabani A, Li Y, Normand S, Stroher U, Tipples GA, Tyler S, Vogrig R, Ward D, Watson B, Brunham RC, Krajden M, Petric M, Skowronski DM, Upton C, Roper RL.** 2003. The Genome sequence of the SARS-associated coronavirus. Science (New York, NY) **300:**1399-1404.
4. **Li W, Moore MJ, Vasilieva N, Sui J, Wong SK, Berne MA, Somasundaran M, Sullivan JL, Luzuriaga K, Greenough TC, Choe H, Farzan M.** 2003. Angiotensin-converting enzyme 2 is a functional receptor for the SARS coronavirus. Nature **426:**450-454.
5. **Rota PA, Oberste MS, Monroe SS, Nix WA, Campagnoli R, Icenogle JP, Peñaranda S, Bankamp B, Maher K, Chen M-H, Tong S, Tamin A, Lowe L, Frace M, DeRisi JL, Chen Q, Wang D, Erdman DD, Peret TCT, Burns C, Ksiazek TG, Rollin PE, Sanchez A, Liffick S, Holloway B, Limor J, McCaustland K, Olsen-Rasmussen M, Fouchier R, Günther S, Osterhaus ADME, Drosten C, Pallansch MA, Anderson LJ, Bellini WJ.** 2003. Characterization of a novel coronavirus associated with severe acute respiratory syndrome. Science (New York, NY) **300:**1394-1399.
6. **Frieman M, Yount B, Heise M, Kopecky-Bromberg SA, Palese P, Baric RS.** 2007. Severe acute respiratory syndrome coronavirus ORF6 antagonizes STAT1 function by sequestering nuclear import factors on the rough endoplasmic reticulum/Golgi membrane. J Virol **81:**9812-9824.
7. **Kopecky-Bromberg SA, Martínez-Sobrido L, Frieman M, Baric RA, Palese P.** 2007. Severe acute respiratory syndrome coronavirus open reading frame (ORF) 3b, ORF 6, and nucleocapsid proteins function as interferon antagonists. J Virol **81:**548-557.

8. **Wathelet MG, Orr M, Frieman MB, Baric RS.** 2007. Severe acute respiratory syndrome coronavirus evades antiviral signaling: role of nsp1 and rational design of an attenuated strain. J Virol **81:**11620-11633.
9. **Nelson CA, Pekosz A, Lee CA, Diamond MS, Fremont DH.** 2005. Structure and Intracellular Targeting of the SARS-Coronavirus Orf7a Accessory Protein. Structure **13:**75-85.
10. **Pekosz A, Schaecher SR, Diamond MS, Fremont DH.** 2006. Structure, expression, and intracellular localization of the SARS-CoV accessory proteins 7a and 7b. The Nidoviruses.
11. **Frieman MB, Yount B, Sims AC, Deming DJ, Morrison TE, Sparks J, Denison M, Heise M, Baric RS.** 2006. SARS coronavirus accessory ORFs encode luxury functions. Advances in experimental medicine and biology **581:**149-152.
12. **Yount B, Roberts RS, Sims AC, Deming D, Frieman MB, Sparks J, Denison MR, Davis N, Baric RS.** 2005. Severe acute respiratory syndrome coronavirus group-specific open reading frames encode nonessential functions for replication in cell cultures and mice. J Virol **79:**14909-14922.
13. **Schaecher SR, Touchette E, Schriewer J, Buller RM, Pekosz A.** 2007. Severe Acute Respiratory Syndrome Coronavirus Gene 7 Products Contribute to Virus-Induced Apoptosis. J Virol **81:**11054-11068.
14. **Tan Y-J, Fielding BC, Goh P-Y, Shen S, Tan THP, Lim SG, Hong W.** 2004. Overexpression of 7a, a Protein Specifically Encoded by the Severe Acute Respiratory Syndrome Coronavirus, Induces Apoptosis via a Caspase-Dependent Pathway. J Virol **78:**14043-14047.
15. **Tan Y-X, Tan THP, Lee MJR, Tham P-Y, Gunalan V, Druce J, Birch C, Catton M, Fu NY, Yu VC, Tan Y-J.** 2007. Induction of apoptosis by the severe acute respiratory syndrome coronavirus 7a protein is dependent on its interaction with the Bcl-XL protein. J Virol **81:**6346-6355.
16. **Tang X, Li G, Vasilakis N, Zhang Y, Shi Z, Zhong Y, Wang L-F, Zhang S.** 2009. Differential stepwise evolution of SARS coronavirus functional proteins in different host species. BMC evolutionary biology **9:**52.
17. **Goto T, Kennel SJ, Abe M, Takishita M, Kosaka M, Solomon A, Saito S.** 1994. A novel membrane antigen selectively expressed on terminally differentiated human B cells. Blood **84:**1922-1930.
18. **Ishikawa J, Kaisho T, Tomizawa H, Lee BO, Kobune Y, Inazawa J, Oritani K, Itoh M, Ochi T, Ishihara K, Hirano T.** 1995. Molecular cloning and chromosomal mapping of a bone marrow stromal cell surface gene, BST2, that may be involved in pre-B-cell growth. Genomics **26:**527-534.
19. **Blasius AL, Giurisato E, Cella M, Schreiber RD, Shaw AS, Colonna M.** 2006. Bone marrow stromal cell antigen 2 is a specific marker of type I IFN-producing cells in the naive mouse, but a promiscuous cell surface antigen following IFN stimulation. Journal of immunology (Baltimore, Md. : 1950) **177:**3260-3265.
20. **Kupzig S, Korolchuk V, Rollason R, Sugden A, Wilde A, Banting G.** 2003. Bst-2/HM1.24 Is a Raft-Associated Apical Membrane Protein with an Unusual Topology. Traffic **4:**694-709.

21. **Ohtomo T, Sugamata Y, Ozaki Y, Ono K, Yoshimura Y, Kawai S, Koishihara Y, Ozaki S, Kosaka M, Hirano T, Tsuchiya M.** 1999. Molecular Cloning and Characterization of a Surface Antigen Preferentially Overexpressed on Multiple Myeloma Cells. Biochemical and biophysical research communications **258:**583-591.
22. **Swiecki M, Scheaffer SM, Allaire M, Fremont DH, Colonna M, Brett TJ.** 2011. Structural and biophysical analysis of BST-2/tetherin ectodomains reveals an evolutionary conserved design to inhibit virus release. The Journal of biological chemistry **286:**2987-2997.
23. **Jones PH, Maric M, Madison MN, Maury W, Roller RJ, Okeoma CM.** 2013. BST-2/tetherin-mediated restriction of chikungunya (CHIKV) VLP budding is counteracted by CHIKV non-structural protein 1 (nsP1). Virology **438:**37-49.
24. **Radoshitzky SR, Dong L, Chi X, Clester JC, Retterer C, Spurgers K, Kuhn JH, Sandwick S, Ruthel G, Kota K, Boltz D, Warren T, Kranzusch PJ, Whelan SPJ, Bavari S.** 2010. Infectious Lassa virus, but not filoviruses, is restricted by BST-2/tetherin. J Virol **84:**10569-10580.
25. **Blondeau C, Pelchen-Matthews A, Mlcochova P, Marsh M, Milne RSB, Towers GJ.** 2013. Tetherin Restricts Herpes Simplex Virus Type 1 and is Antagonised by Glycoprotein M. J Virol.
26. **Bampi C, Rasga L, Roux L.** 2013. Antagonism to human BST-2/tetherin by Sendai virus glycoproteins. J Gen Virol **94:**1211-1219.
27. **Neil SJD, Zang T, Bieniasz PD.** 2008. Tetherin inhibits retrovirus release and is antagonized by HIV-1 Vpu. Nature **451:**425-430.
28. **Fitzpatrick K, Skasko M, Deerinck TJ, Crum J, Ellisman MH, Guatelli J.** 2010. Direct restriction of virus release and incorporation of the interferon-induced protein BST-2 into HIV-1 particles. PLoS pathogens **6:**e1000701.
29. **Perez-Caballero D, Zang T, Ebrahimi A, McNatt MW, Gregory DA, Johnson MC, Bieniasz PD.** 2009. Tetherin Inhibits HIV-1 Release by Directly Tethering Virions to Cells. Cell **139:**499-511.
30. **Andrew AJ, Miyagi E, Kao S, Strebel K.** 2009. The formation of cysteine-linked dimers of BST-2/tetherin is important for inhibition of HIV-1 virus release but not for sensitivity to Vpu. Retrovirology.
31. **Galão RP, Le Tortorec A, Pickering S, Kueck T, Neil SJD.** 2012. Innate Sensing of HIV-1 Assembly by Tetherin Induces NFκB-Dependent Proinflammatory Responses. Cell host & microbe **12:**633-644.
32. **Douglas JL, Viswanathan K, McCarroll MN, Gustin JK, Früh K, Moses AV.** 2009. Vpu Directs the Degradation of the Human Immunodeficiency Virus Restriction Factor BST-2/Tetherin via a βTrCP-Dependent Mechanism. J Virol **83:**7931-7947.
33. **Mangeat B, Gers-Huber G, Lehmann M, Zufferey M, Luban J, Piguet V.** 2009. HIV-1 Vpu Neutralizes the Antiviral Factor Tetherin/BST-2 by Binding It and Directing Its Beta-TrCP2-Dependent Degradation. PLoS pathogens **5:**e1000574.
34. **Mitchell RS, Katsura C, Skasko MA, Fitzpatrick K, Lau D, Ruiz A, Stephens EB, Margottin-Goguet F, Benarous R, Guatelli JC.** 2009. Vpu Antagonizes

BST-2–Mediated Restriction of HIV-1 Release via β-TrCP and Endo-Lysosomal Trafficking. PLoS pathogens **5:**e1000450.

35. **Gupta RK, Mlcochova P, Pelchen-Matthews A, Petit SJ, Mattiuzzo G, Pillay D, Takeuchi Y, Marsh M, Towers GJ.** 2009. Simian immunodeficiency virus envelope glycoprotein counteracts tetherin/BST-2/CD317 by intracellular sequestration. Proceedings of the National Academy of Sciences of the United States of America **106:**20889-20894.

36. **Le Tortorec A, Neil SJ.** 2009. Antagonism to and intracellular sequestration of human tetherin by the human immunodeficiency virus type 2 envelope glycoprotein. J Virol **83:**11966-11978.

37. **Wang S-M, Huang K-J, Wang C-T.** 2014. BST2/CD317 counteracts human coronavirus 229E productive infection by tethering virions at the cell surface. Virology **449:**287-296.

38. **Zhang F, Wilson SJ, Landford WC, Virgen B, Gregory D, Johnson MC, Munch J, Kirchhoff F, Bieniasz PD, Hatziioannou T.** 2009. Nef Proteins from Simian Immunodeficiency Viruses Are Tetherin Antagonists. Cell host & microbe **6:**54-67.

39. **Kaletsky RL, Francica JR, Agrawal-Gamse C, Bates P.** 2009. Tetherin-mediated restriction of filovirus budding is antagonized by the Ebola glycoprotein. Proceedings of the National Academy of Sciences of the United States of America **106:**2886-2891.

40. **Stertz S, Reichelt M, Spiegel M, Kuri T, Martínez-Sobrido L, García-Sastre A, Weber F, Kochs G.** 2007. The intracellular sites of early replication and budding of SARS-coronavirus. Virology **361:**304-315.

41. **Yount B, Curtis KM, Fritz EA, Hensley LE, Jahrling PB, Prentice E, Denison MR, Geisbert TW, Baric RS.** 2003. Reverse genetics with a full-length infectious cDNA of severe acute respiratory syndrome coronavirus. Proceedings of the National Academy of Sciences of the United States of America **100:**12995-13000.

42. **Sims AC, Baric RS, Yount B, Burkett SE, Collins PL, Pickles RJ.** 2005. Severe acute respiratory syndrome coronavirus infection of human ciliated airway epithelia: role of ciliated cells in viral spread in the conducting airways of the lungs. J Virol **79:**15511-15524.

43. **Pewe L, Zhou H, Netland J, Tangudu C, Olivares H, Shi L, Look D, Gallagher T, Perlman S.** 2005. A severe acute respiratory syndrome-associated coronavirus-specific protein enhances virulence of an attenuated murine coronavirus. J Virol **79:**11335-11342.

44. **Tangudu C, Olivares H, Netland J, Perlman S, Gallagher T.** 2007. Severe acute respiratory syndrome coronavirus protein 6 accelerates murine coronavirus infections. J Virol **81:**1220-1229.

45. **Frieman M, Ratia K, Johnston RE, Mesecar AD, Baric RS.** 2009. Severe acute respiratory syndrome coronavirus papain-like protease ubiquitin-like domain and catalytic domain regulate antagonism of IRF3 and NF-kappaB signaling. J Virol **83:**6689-6705.

46. **Frieman M, Yount B, Heise M, Kopecky-Bromberg SA, Palese P, Baric RS.** 2007. Severe acute respiratory syndrome coronavirus ORF6 antagonizes

STAT1 function by sequestering nuclear import factors on the rough endoplasmic reticulum/Golgi membrane. J Virol **81:**9812-9824.

47. **Barretto N, Jukneliene D, Ratia K, Chen Z, Mesecar AD, Baker SC.** 2005. The papain-like protease of severe acute respiratory syndrome coronavirus has deubiquitinating activity, p. 15189-15198, J Virol, vol. 79.

48. **Clementz MA, Chen Z, Banach BS, Wang Y, Sun L, Ratia K, Baez-Santos YM, Wang J, Takayama J, Ghosh AK, Li K, Mesecar AD, Baker SC.** 2010. Deubiquitinating and interferon antagonism activities of coronavirus papain-like proteases. J Virol **84:**4619-4629.

49. **Wathelet MG, Orr M, Frieman MB, Baric RS.** 2007. Severe acute respiratory syndrome coronavirus evades antiviral signaling: role of nsp1 and rational design of an attenuated strain. J Virol **81:**11620-11633.

50. **Kamitani W, Narayanan K, Huang C, Lokugamage K, Ikegami T, Ito N, Kubo H, Makino S.** 2006. Severe acute respiratory syndrome coronavirus nsp1 protein suppresses host gene expression by promoting host mRNA degradation., p. 12885-12890, Proc. Natl. Acad. Sci. U.S.A., vol. 103.

51. **Kopecky-Bromberg SA, Martinez-Sobrido L, Frieman M, Baric RA, Palese P.** 2007. Severe acute respiratory syndrome coronavirus open reading frame (ORF) 3b, ORF 6, and nucleocapsid proteins function as interferon antagonists. J Virol **81:**548-557.

52. **Devaraj SG, Wang N, Chen Z, Chen Z, Tseng M, Barretto N, Lin R, Peters CJ, Tseng CT, Baker SC, Li K.** 2007. Regulation of IRF-3-dependent innate immunity by the papain-like protease domain of the severe acute respiratory syndrome coronavirus, p. 32208-32221, J Biol Chem, vol. 282.

53. **Basu D, Walkiewicz MP, Frieman M, Baric RS, Auble DT, Engel DA.** 2009. Novel influenza virus NS1 antagonists block replication and restore innate immune function. J Virol **83:**1881-1891.

54. **Frieman M, Ratia K, Johnston RE, Mesecar AD, Baric RS.** 2009. Severe acute respiratory syndrome coronavirus papain-like protease ubiquitin-like domain and catalytic domain regulate antagonism of IRF3 and NF-kappaB signaling. J Virol **83:**6689-6705.

55. **Kamitani W, Narayanan K, Huang C, Lokugamage K, Ikegami T, Ito N, Kubo H, Makino S.** 2006. Severe acute respiratory syndrome coronavirus nsp1 protein suppresses host gene expression by promoting host mRNA degradation. PNAS **103:**12885-12890.

56. **Van Damme N, Goff D, Katsura C, Jorgenson RL, Mitchell R, Johnson MC, Stephens EB, Guatelli J.** 2008. The interferon-induced protein BST-2 restricts HIV-1 release and is downregulated from the cell surface by the viral Vpu protein. Cell host & microbe **3:**245-252.

57. **Hoa XD, Kirk AG, Tabrizian M.** 2007. Towards integrated and sensitive surface plasmon resonance biosensors: a review of recent progress. Biosensors & bioelectronics **23:**151-160.

58. **McNatt MW, Zang T, Hatziioannou T, Bartlett M, Ben Fofana I, Johnson WE, Neil SJD, Bieniasz PD.** 2009. Species-Specific Activity of HIV-1 Vpu and Positive Selection of Tetherin Transmembrane Domain Variants. PLoS pathogens **5:**e1000300.

59. **Mansouri M, Viswanathan K, Douglas JL, Hines J, Gustin J, Moses AV, Früh K.** 2009. Molecular mechanism of BST2/tetherin downregulation by K5/MIR2 of Kaposi's sarcoma-associated herpesvirus. J Virol **83:**9672-9681.

60. **Jia HP, Look DC, Shi L, Hickey M, Pewe L, Netland J, Farzan M, Wohlford-Lenane C, Perlman S, McCray PB, Jr.** 2005. ACE2 receptor expression and severe acute respiratory syndrome coronavirus infection depend on differentiation of human airway epithelia. J Virol **79:**14614-14621.

Figure 1

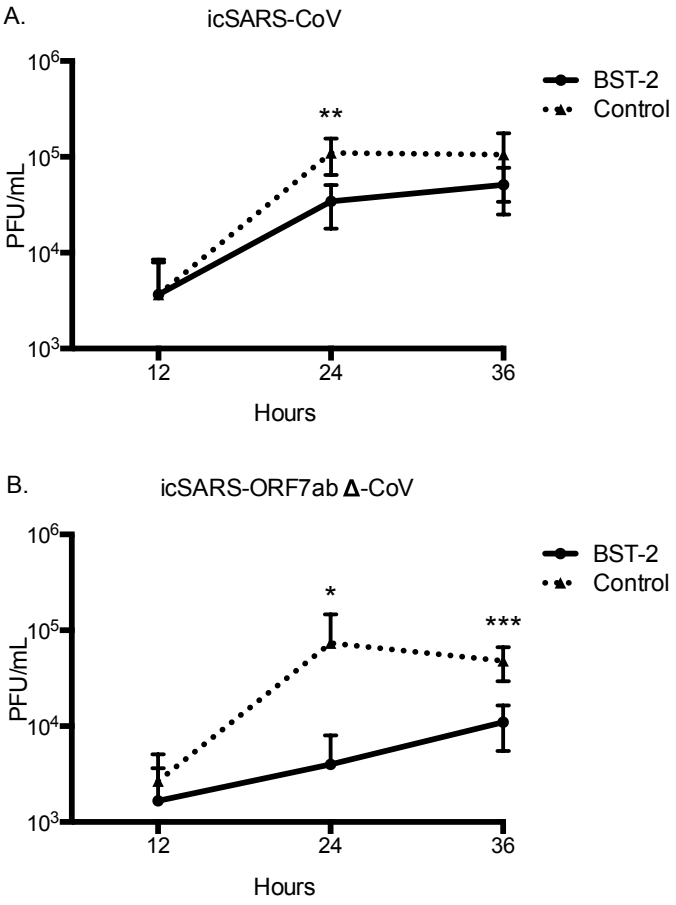

Figure 2

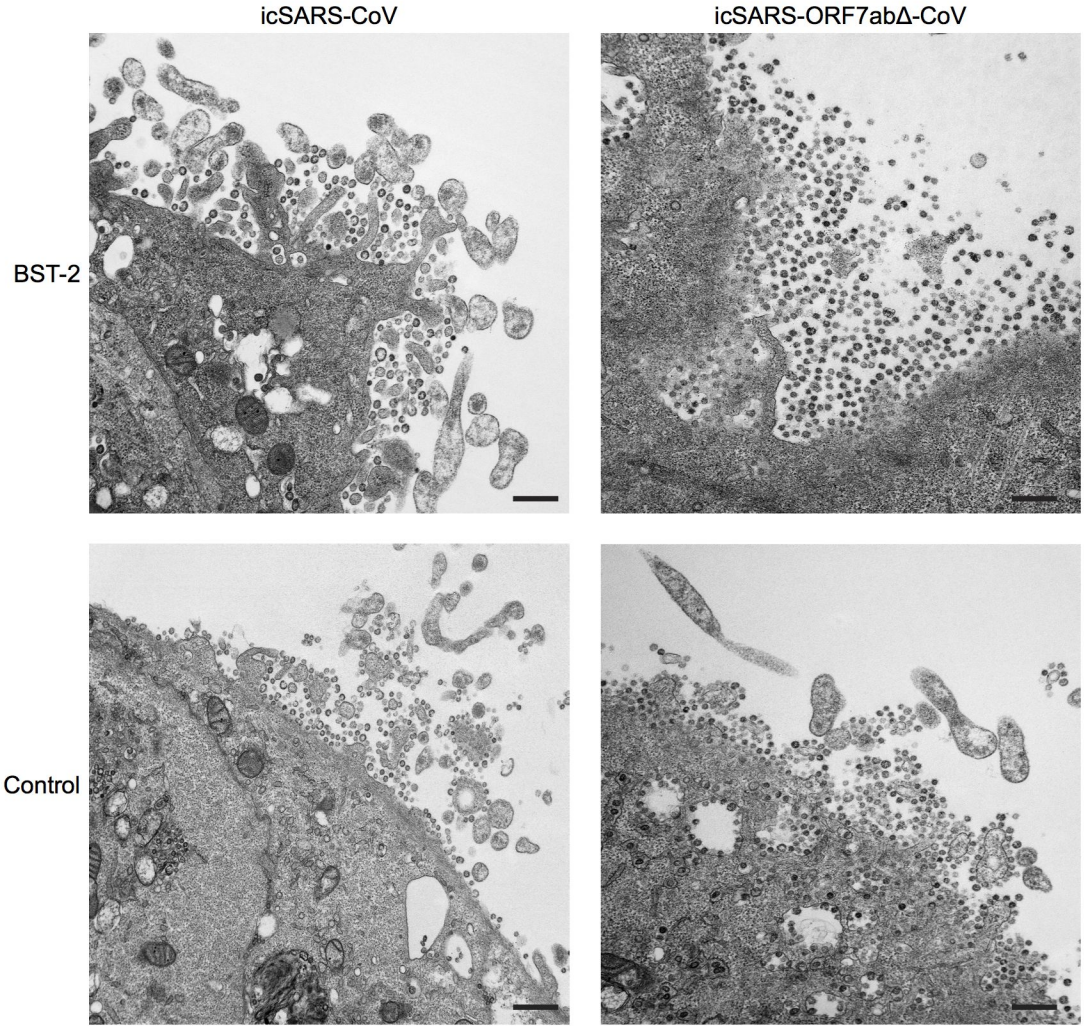

Figure 3

A.

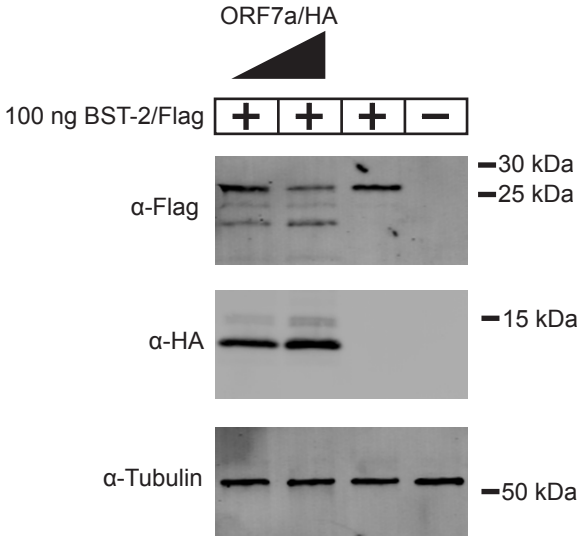

B.

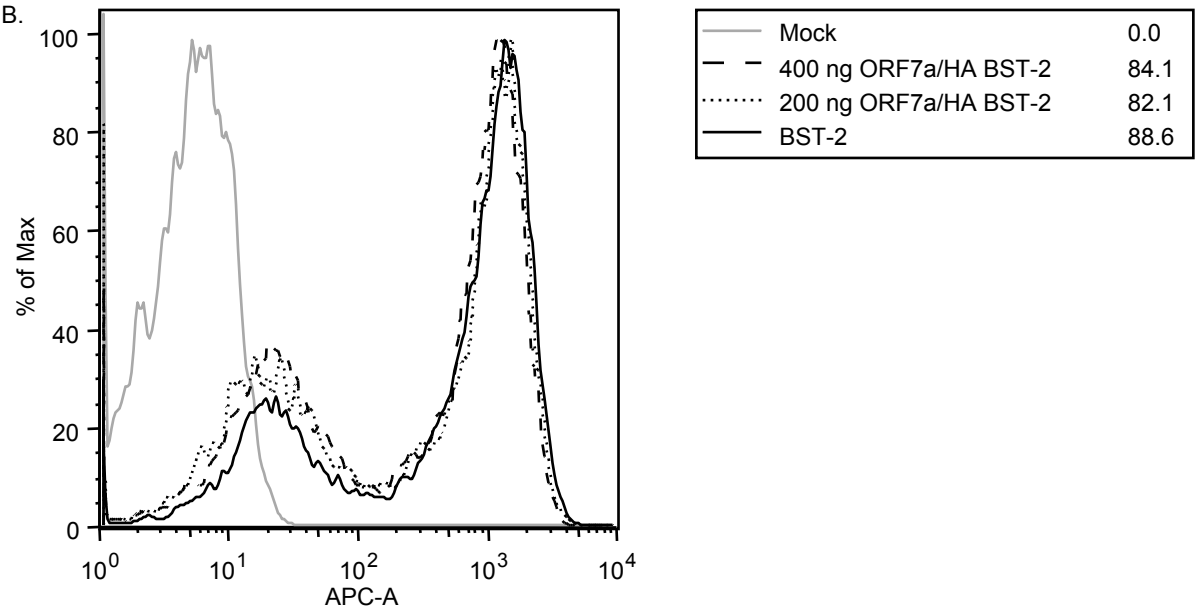

Figure 4

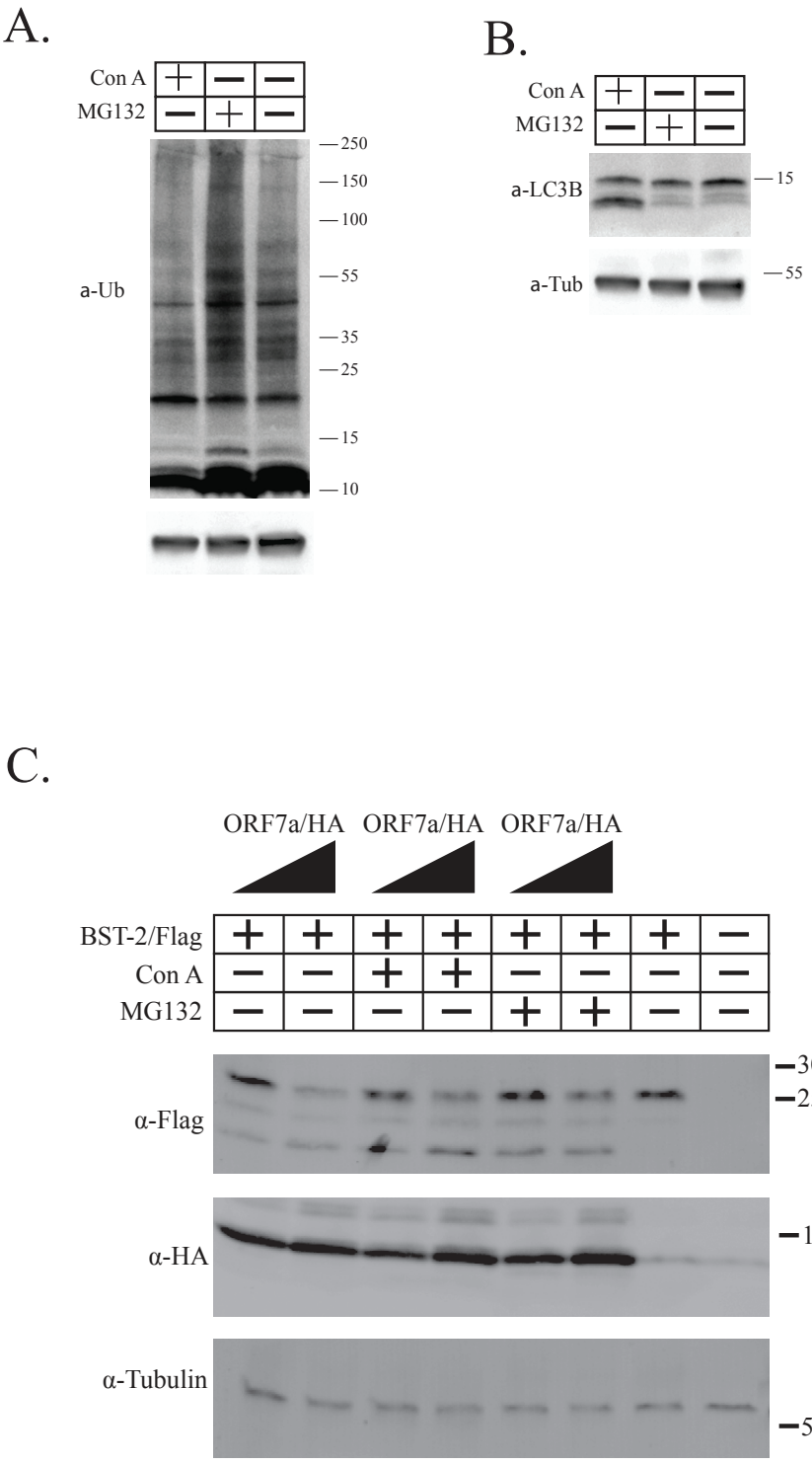

Figure 5

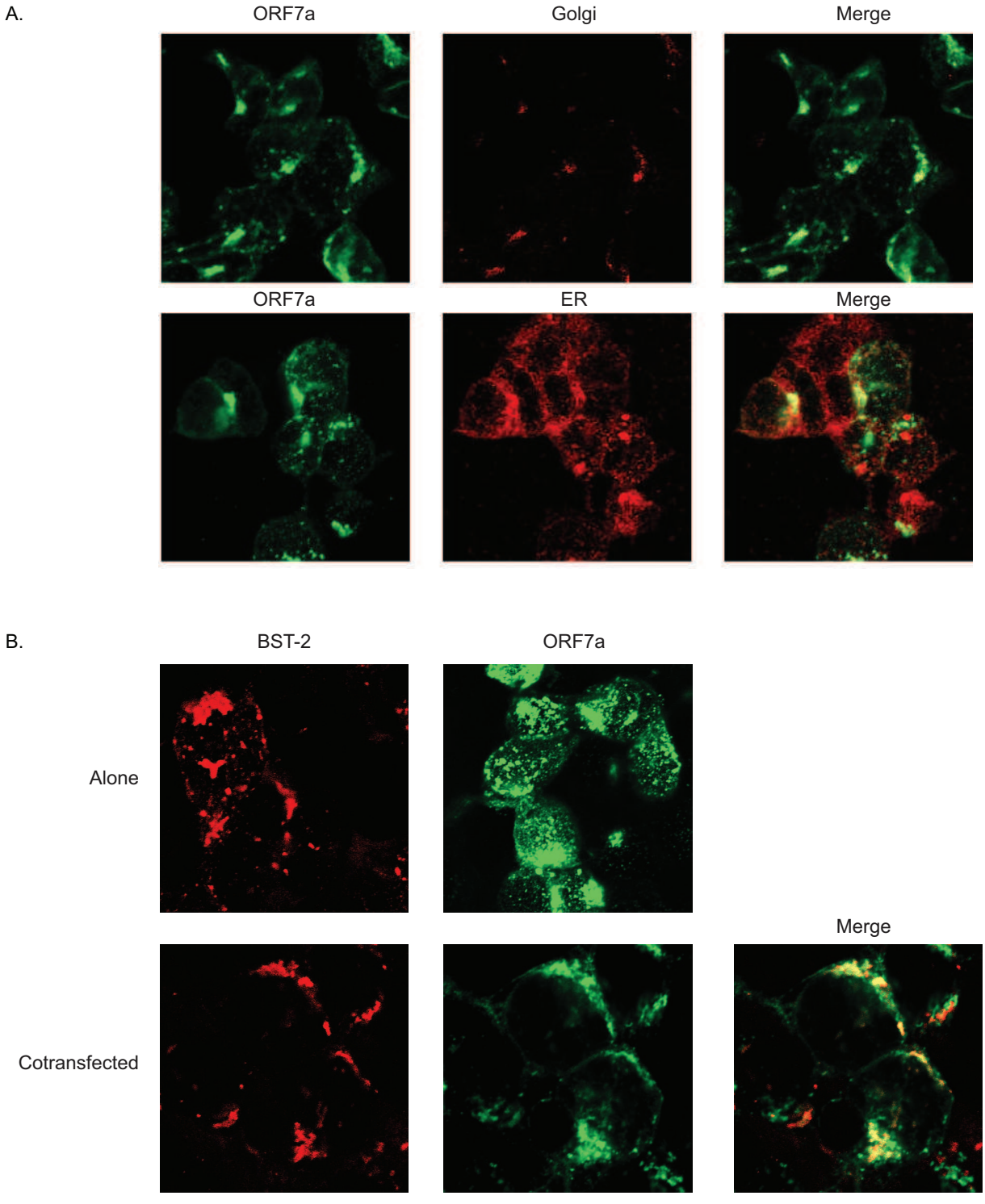

Figure 6

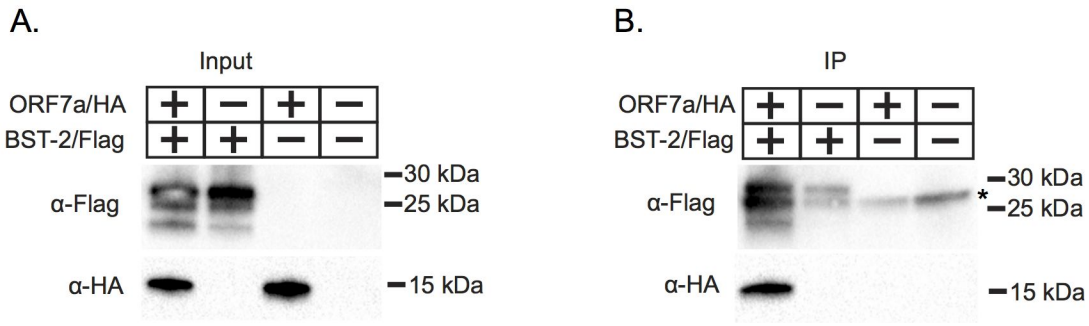

Figure 7

A.

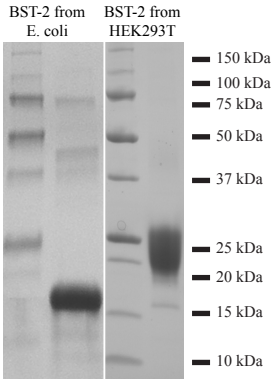

B.

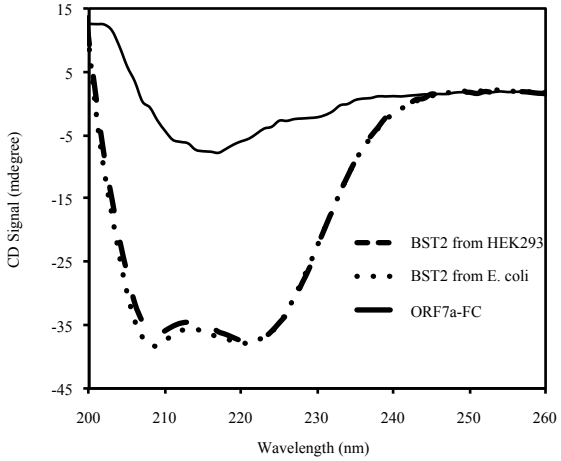

C.

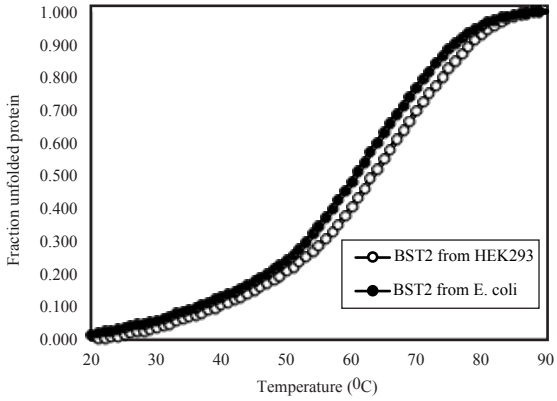

D.

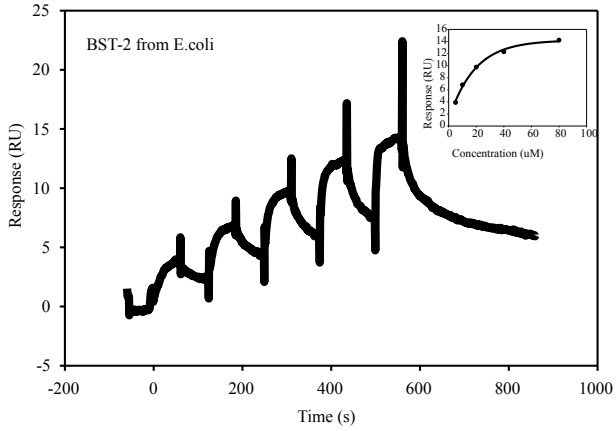

E.

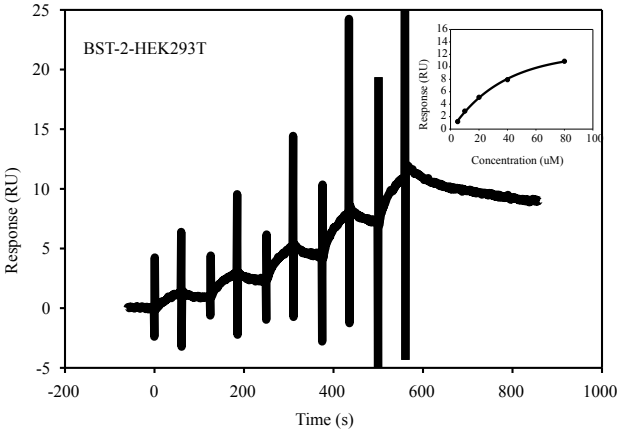

Figure 8

A.

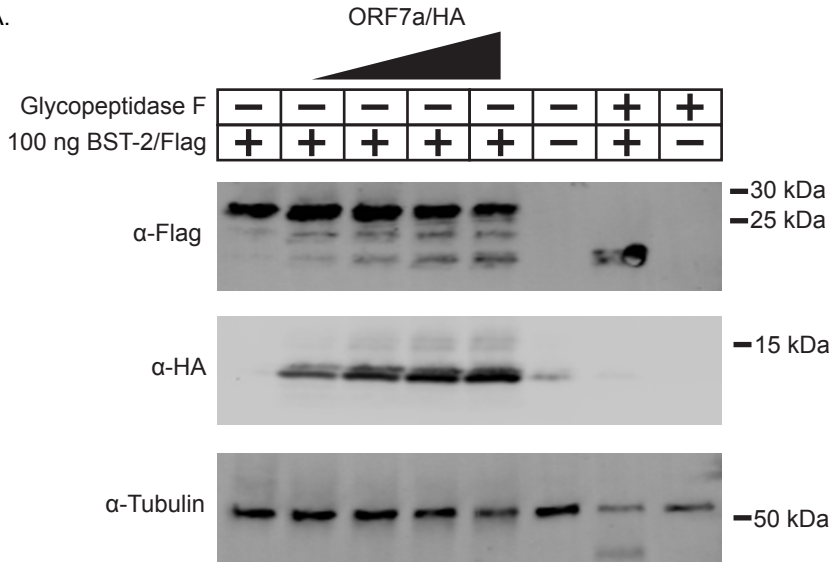

B.

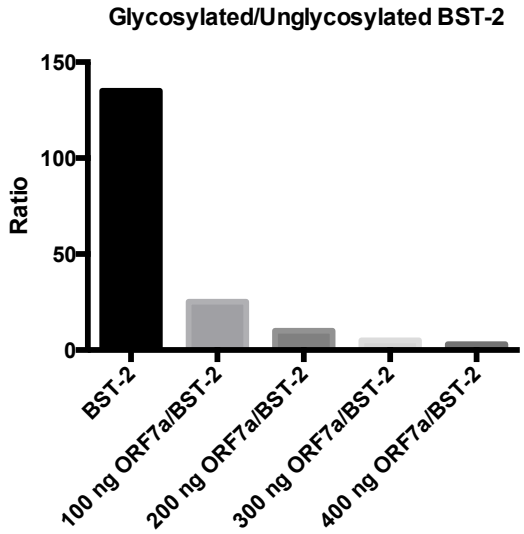

Figure 9

A.

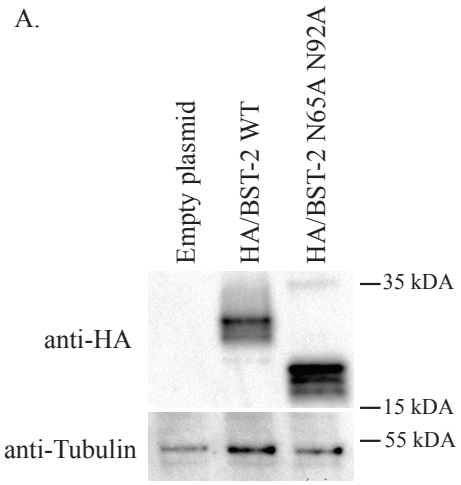

B.

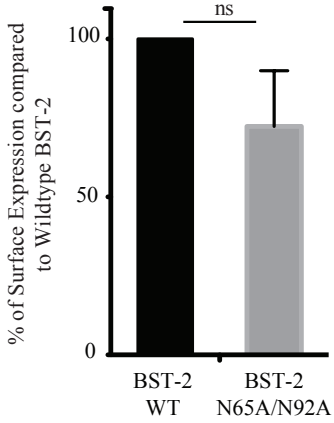

C.